NASA TM-88222

NASA Technical Memorandum 88222

NASA-TM-88222 19860018904

# Numerical Simulation of Boundary Layers: Part 1. Weak Formulation and Numerical Method

Philippe R. Spalart

February 1986

LIBRARY COPY

FEB 1 8 1986

LANGLEY RESEARCH CENTER
LIBRARY, NASA
HAMPTON, VIRGINIA

NF00939

FOR REFERENCE

NOT TO BE TAKEN FROM THIS ROOM

NASA
National Aeronautics and
Space Administration

NASA Technical Memorandum 88222

# Numerical Simulation of Boundary Layers: Part 1. Weak Formulation and Numerical Method

Philippe R. Spalart, Ames Research Center, Moffett Field, California

February 1986

National Aeronautics and
Space Administration

**Ames Research Center**
Moffett Field, California 94035

N86-28376#

# Numerical simulation of boundary layers

## Part 1. Weak formulation and numerical method

By PHILIPPE R. SPALART

NASA Ames Research Center, Moffett Field, California 94035

A numerical method designed to solve the time-dependent, three-dimensional, incompressible Navier-Stokes equations in boundary layers is presented. The fluid domain is the half-space over a flat plate, and periodic conditions are applied in the horizontal directions. The discretization is spectral. The basis functions are divergence-free and a weak formulation of the momentum equation is used, which eliminates the pressure term. An exponential mapping and Jacobi polynomials are used in the semi-infinite direction, with the irrotational component receiving special treatment. Issues related to the accuracy, stability and efficiency of the method are discussed. Very fast convergence is demonstrated on some model problems with smooth solutions. The method has also been shown to accurately resolve the fine scales of transitional and turbulent boundary layers.

## 1. Introduction

The state of the art in "direct" and "large-eddy" numerical simulations of turbulent flows is reviewed by Rogallo & Moin (1984). These simulations, in which the energy-containing structures are computed, have contributed to the understanding of several turbulent flows: isotropic turbulence, homogeneous turbulence with mean strain, shear or rotation, plane channel and curved channel flows. The results can also be used to accurately calibrate existing turbulence models, or suggest new models. While limited to simple geometries, relatively low Reynolds numbers and small statistical samples, direct numerical studies have the advantage of providing much more complete information than experiments can provide. Numerical simulations are also useful in the study of transition (Orszag & Kells 1980, Wray & Hussaini 1984), even though the final stages of transition have not yet been computed for lack of numerical resolution.

Both the numerical methods and the "supercomputers" are rapidly improving. The numerical methods used are in general spectral, at least in the periodic directions. Spectral methods are the most efficient in terms of resolving fine structures with a given number of degrees of freedom (Gottlieb & Orszag 1977). They also have very high, "infinite-order" formal accuracy. Homogeneous turbulence was first simulated, with periodic conditions and Fourier series in all directions. This method is well established and major improvements are unlikely to be made. In contrast, many methods are competing for the straight-channel flow (Orszag & Kells 1980, Moin & Kim 1982, Kleiser 1982, Moser *et al.* 1983).

A few methods exist for free mixing layers (Cain *et al.* 1984), curved channels (Moser *et al.* 1983, Marcus 1984), pipe flow (Leonard & Wray 1982), and boundary layers (Orszag & Patera 1983, Wray & Hussaini 1984).

This paper is the first of three on the direct simulation of boundary layers. Transition simulations are presented in Part 2, and simulations of fully developed turbulence and relaminarization are presented in Part 3. The purpose of Part 1 is to present a spectral numerical method designed specifically for the simulation of boundary layers, to discuss certain issues regarding accuracy and efficiency, and to report on tests the method was subjected to. Two major items are the weak formulation, which applies to other flows, and the choice of the mapping and basis functions, which is specific to the boundary layer. Preliminary results were presented by Spalart (1984a, 1984b) and Spalart & Leonard (1985). In the design of major computing projects, considerations of physical relevance and of computational efficiency are taken into account and sometimes conflict. For this project, periodic conditions were adopted in both the spanwise and streamwise directions. Such conditions are optimal in terms of efficiency and will be taken for granted in this paper. Their physical implications will be discussed in Parts 2 and 3.

## 2. Weak formulation.

Leonard (1981) presented a spectral method based on divergence-free basis functions and a weak formulation of the incompressible Navier-Stokes equations. He mentioned the following advantages over previous methods: exact treatment of the continuity condition and boundary conditions, simpler time-advance scheme (the pressure term is eliminated), and lower memory requirements. The method has most of the advantages of the vorticity-stream function methods, but by working with the velocity instead of the vorticity it avoids the well-known problem of having to prescribe vorticity boundary conditions. A weak formulation is used because it is consistent with the use of constrained basis functions, not because weak solutions are expected. The method was successfully applied to a circular pipe by Leonard & Wray (1982) and to straight and curved channels by Moser *et al.* (1983).

The present method uses Leray's weak formulation of the equations, which is slightly different from Leonard's. Leray's formulation was presented in 1933 and has been used extensively for theoretical studies of the equations (Ladyzhenskaya 1969, Heywood 1980, Temam 1983) and with finite-element numerical methods, but apparently not with spectral methods. The relative merits of these two formulations will be discussed.

### 2.1. *Leonard's formulation*

The incompressible Navier-Stokes equations are written

$$\nabla.\mathbf{U} = 0, \tag{1}$$

$$\mathbf{U}_t + \mathbf{U}.\nabla\mathbf{U} = -\nabla p + \nu\nabla^2\mathbf{U} + \mathbf{f}, \tag{2}$$

where $\mathbf{U} = (u, v, w)$ is the velocity vector, $\nabla$ the gradient operator, $t$ the time, $p$ the pressure, and $\nu$ the kinematic viscosity. The density, being uniform, can be set to 1 and omitted. The term $\mathbf{f}$ may be either a forcing term, or an extra term (function of $\mathbf{U}$). Such terms will appear in the equation (see Parts 2 and 3). However they do not interfere with the formulation, and can be omitted for the moment.

The boundary conditions at a solid wall ($y = 0$ in this case) are the viscous conditions

$$\mathbf{U}(x, 0, z) = 0. \tag{3}$$

If the domain is infinite, a "free-stream velocity" $\mathbf{U}_\infty$ is prescribed. In the present case it is approached for large values of $y$

$$\lim_{y \to \infty} \mathbf{U} = \mathbf{U}_\infty. \tag{4}$$

The rate at which $\mathbf{U}$ tends to $\mathbf{U}_\infty$ may have to be prescribed also; existence and uniqueness questions in infinite domains are delicate (Heywood 1980).

The momentum equation (2) governs the time-evolution of the velocity field under the constraints of the continuity condition (1) and the boundary conditions (3,4). These constraints are linear and time-independent; they define a subspace of the vector space of all possible velocity fields. The idea is to restrict the search for a solution to that subspace from the onset. Numerically, the first advantage is that by working inside a smaller space one has fewer degrees of freedom to follow for a given level of resolution: two per mode, instead of four when the three velocity components and the pressure are used (Leonard 1981).

Once the continuity condition (1) has been applied the description acquires a non-local character; the different velocity components, at different points, are coupled. This reflects the instantaneous interactions, through the pressure, that characterize incompressible flows. It is then natural to apply the momentum equation, not locally and separately for the three velocity components, but in a global sense. This is done by taking the dot product of the vector equation (2) and suitably chosen vector "test" functions, and integrating over the entire domain. The inner product $< \mathbf{U}_1, \mathbf{U}_2 >$ of two vector functions is defined by

$$< \mathbf{U}_1, \mathbf{U}_2 > \equiv \int\int\int \mathbf{U}_1.\mathbf{U}_2 \quad dx \quad dy \quad dz. \tag{5}$$

Let $\mathbf{V}$ be a test function. The product of (2) with $\mathbf{V}$ is

$$< \mathbf{U}_t, \mathbf{V} > + < \mathbf{U}.\nabla\mathbf{U}, \mathbf{V} > = - < \nabla p, \mathbf{V} > + < \nu\nabla^2\mathbf{U}, \mathbf{V} > . \tag{6}$$

Leonard used test functions $\mathbf{V}$ that satisfy the divergence-free condition (1) and have zero normal velocity at the walls (they satisfy only the $y$ component of (3)). An integration by parts then shows that $< \nabla p, \mathbf{V} > = 0$; the pressure term is eliminated. Actually, any gradient-type term is orthogonal to $\mathbf{V}$ in the sense of $< .,. >$. Considering the well-known identity $\mathbf{U}.\nabla\mathbf{U} = \nabla(|\mathbf{U}|^2/2) - \mathbf{U} \times \omega$, where $\omega$ is the vorticity vector, one has the choice of keeping $\mathbf{U}.\nabla\mathbf{U}$ or just $-\mathbf{U} \times \omega$ for the transport term. Leonard arrived at the equation

$$< \mathbf{U}, \mathbf{V} >_t - < \mathbf{U} \times \omega, \mathbf{V} > = \nu < \nabla^2\mathbf{U}, \mathbf{V} > . \tag{7}$$

This equation will be advanced step by step in time, and no constraints need to be applied. While the system (1-4) was an initial-boundary-value problem, (7) is an initial-value problem, and is easier to integrate in time. In addition (1) and (3) are satisfied exactly, which is not always the case with other methods.

### 2.2. *Leray's formulation*

In Leonard's formulation, the test-function space is larger than the basis-function space, because it is defined by fewer constraints (the basis functions satisfy all three components of (3)). The test-function space is only "slightly" larger, in the sense that the basis-function space is dense in it for the norm defined by (5). However, in a numerical context, when finite-dimensional subspaces are used, the difference is significant. In Leray's formulation, the test functions satisfy both the normal and the tangential components of (3); the two spaces are the same. One has a true least-squares method. Leray's test-function space has the advantage of being the smallest set of test functions sufficient to govern the evolution of $\mathbf{U}$; within that space the bilinear symmetric form $< .,. >$ is positive-definite. Numerically, the advantage is that the choice of the test functions will be unique once the basis functions have been chosen, and that the matrix representing $< .,. >$ will be symmetric.

The extra constraint on $\mathbf{V}$ also allows one to integrate the viscous term by parts, and to arrive at

$$< \mathbf{U}, \mathbf{V} >_t - < \mathbf{U} \times \omega, \mathbf{V} >= -\nu < \nabla \mathbf{U}, \nabla \mathbf{V} > . \tag{8}$$

Thus the viscous operator is also symmetric, and is negative-definite. This has some computational advantages (lower storage, use of the Cholesky decomposition, simultaneous diagonalization of the two operators), and it guarantees that the numerical Stokes eigenvalues will be real and negative.

Another issue is the conservation of energy. The contribution of the transport term to the global kinetic energy $< \mathbf{U}, \mathbf{U} > /2$ of the numerical solution should, ideally, be 0. With Leray's formulation (the expansion and test functions being the same) $\mathbf{U}$ can be constructed as a linear combination of test functions. Thus if (8) is satisfied for every $\mathbf{V}$, one also has, by linear combination,

$$\frac{1}{2} < \mathbf{U}, \mathbf{U} >_t - < \mathbf{U} \times \omega, \mathbf{U} >= -\nu < \nabla \mathbf{U}, \nabla \mathbf{U} > . \tag{9}$$

The contribution of the transport term, $< \mathbf{U} \times \omega, \mathbf{U} >$, is 0 since $(\mathbf{U} \times \omega)$ and $\mathbf{U}$ are orthogonal at every point. Thus the global energy of an inviscid flow is conserved by the spatial discretization. Errors in the time integration may still affect the energy, so that one sometimes speaks of "semiconservation" of energy. However, this semiconservation property and the use of an adequate time-integration scheme will ensure that the numerical solution remains stable. Equation (9) also shows that the contribution of the viscous term is negative, as expected. In Leonard's method, semiconservation of energy does not seem to hold; however, he does not report any stability problems.

The disadvantage of Leray's formulation, in a numerical context, is that Chebyshev polynomials cannot be used to treat the wall-bounded direction, for the reason that these polynomials are orthogonal with respect to a weight function, $(1-y^2)^{-1/2}$, which is singular at the wall. Moser *et al.* used Chebyshev polynomials to construct the basis functions and the same polynomials, multiplied by $(1-y^2)^{-1/2}$, to construct the test functions. Thus the two families are orthogonal to each other with respect to the $< .,. >$ product. The test functions are less regular than the basis functions near the wall. In Leray's formulation (the basis functions and test functions being the same) one would have to split the Chebyshev weight function between the basis and test functions. As a result, the functions would have infinite derivatives at the wall, which must be avoided. It is essential for the accuracy of the spectral method to have regular basis functions (Gottlieb & Orszag 1977).

This is the main reason why Jacobi, instead of Chebyshev, polynomials are used here. Leonard & Wray (1982) used Jacobi polynomials partly because they allowed a proper treatment of the polar-coordinate singularity. Numerically, Chebyshev polynomials would be preferable because "fast" Chebyshev transforms can be used. With these fast transforms, the number of operations the computer has to perform is of the order of $N \log(N)$, instead of $N^2$ for a standard transform. The penalty becomes heavy when $N$, the number of polynomials, exceeds about 50. Thus Jacobi-based methods like Leonard and Wray's and the present one are competitive for flows with only one wall, when the value of $N$ is typically between 20 and 40, but are less attractive for channel flows, when $N$ can be as high as 128. There is need for a "fast Jacobi transform."

Leonard's and Leray's formulations are elegant and lend themselves to the design of numerical methods with attractive properties, as will be discussed. On the other hand, the simplicity of the domain shape and the periodicity in two directions are used extensively. It remains to be seen how conveniently this formulation can be applied to more complex domains or to zonal methods.

## 3. Numerical Method

The discretization is spectral in space and of finite-difference type, with second-order accuracy, in time. In addition to their high accuracy, the global character of spectral methods seems to make them especially appropriate for the simulation of incompressible flows, since all the points in the domain are instantly coupled by the pressure interactions.

### 3.1. *Construction of the vector basis functions*

The three-dimensional vector basis functions are constructed as products of one-dimensional functions. In the $x$ and $z$ directions, parallel to the wall, periodic conditions are applied and Fourier series can be used. Let $\mathbf{k} = (k_x, k_z)$ be the wave-vector in the horizontal plane and $k$ denote its norm, $\sqrt{k_x^2 + k_z^2}$. Let $\hat{\mathbf{U}}(k_x, y, k_z)$ denote the Fourier transform of $\mathbf{U}(x, y, z)$. Equation (1) becomes

$$ik_x\hat{u} + \hat{v}_y + ik_z\hat{w} = 0, \tag{10}$$

where $i^2 = -1$. Leonard & Wray (1982) introduced a decomposition into "+" and "−" modes to simplify this equation. The + modes contain the horizontal component of velocity parallel to the wave-vector and the vertical component, and the − modes contain the component orthogonal to the wave-vector: $\hat{u}^+ \equiv (k_x\hat{u} + k_z\hat{w})/k, \quad \hat{u}^- \equiv (k_z\hat{u} - k_x\hat{w})/k$. Equation (10) becomes

$$ik\hat{u}^+ + \hat{v}_y = 0. \tag{11}$$

The − modes are not involved in the continuity equation; they only have to satisfy the boundary conditions. They are decoupled from the + modes in both linear operators in (8). The + modes are two-dimensional modes in the vertical plane containing the wave-vector; the rotation amounts to Squire's transformation (Schlichting 1979).

Thanks to the Fourier transforms and to Leonard and Wray's +/− decomposition the problem of defining vector basis functions is reduced to the problem of defining one-dimensional scalar functions with a single zero at $y = 0$, for $\hat{u}^-$, and functions with a double zero at $y = 0$, for $\hat{v}$. $\hat{u}^+$ is then given by (11). The behavior of the functions as

$y \to \infty$, however, deserves special attention. Leonard & Wray (1982) and Moser *et al* (1983) treated finite domains.

### 3.2. *Choice of the mapping*

Orthogonal polynomials make convenient "building blocks" for numerical methods. As shown by Gottlieb & Orszag (1977) using polynomials directly in terms of $y$ over $[0, \infty]$ is inefficient, essentially because all polynomials diverge as $y \to \infty$. Grosch & Orszag (1977) showed that the procedure of mapping the infinite interval $[0, \infty]$ into a finite interval and using polynomials in terms of the new variable was more efficient than other procedures, including the truncation of $[0, \infty]$ to a large but finite value of $y$. Two obvious candidates are the exponential mapping and the algebraic mapping. Orszag (1976), Grosch & Orszag (1977), and Boyd (1982) all strongly criticized the exponential mapping and recommended algebraic mappings instead, in particular for the boundary-layer problem. Some boundary-layer results using an algebraic mapping are reported by Orszag & Patera (1983). Cain *et al.* (1984) found that a hyperbolic-tangent mapping and Fourier series were efficient in treating the interval $[-\infty, \infty]$ in their study of free shear layers.

The exponential mapping has certain advantages (simpler metric coefficient and differentiation operator, rapid expansion of the collocation points outside the boundary layer) and will be used here. A satisfactory solution was found to Orszag's (1976) objection and the resulting method is believed to be more accurate, for our purposes, than existing methods. Once this mapping has been chosen a certain family of Jacobi polynomials lends itself well to the construction of basis functions that will keep the Stokes operators in (8) narrow-banded.

Let the transformed variable $\eta$ be defined by

$$\eta \equiv e^{-y/y_0}. \tag{12}$$

The parameter $y_0$ is a length scale and will be chosen to be of the order of the boundary-layer thickness. $\eta$ varies over [0,1]. The derivatives of a function $\phi$ satisfy

$$\phi_y = -\frac{\eta}{y_0}\phi_\eta. \tag{13}$$

Thus if $\phi$ is a polynomial in terms of $\eta$, $\phi_y$ is also a polynomial, and of the same degree.

The potential problem with the exponential mapping is the following (Orszag 1976). Far from the plate, the vorticity is assumed to tend to 0. The velocity field is then irrotational as well as divergence-free: it satisfies Laplace's equation. For a Fourier-transformed variable, say $\hat{v}$, Laplace's equation becomes $\hat{v}_{yy} - k^2\hat{v} = 0$ and its solutions are linear combinations of $\exp(ky)$ and $\exp(-ky)$. Only the solution $\exp(-ky)$ satisfies the boundary condition (4). In terms of $\eta$, it is equal to $\eta^{ky_0}$. Now $ky_0$, in practice, often takes values lower than 1, so that the derivatives of $\hat{v}$ with respect to $\eta$ tend to $\infty$ as $\eta \to 0$. Clearly such a function cannot be well approximated by polynomials, so that slow convergence of the numerical method would result. A singularity was introduced by the mapping. The problem can be alleviated by making $y_0$ large in order to bring $ky_0$ above 1 or even higher, but then one is squandering collocation points away from the boundary layer itself. In addition, any noninteger value of $ky_0$ results in unbounded derivatives at high enough order. With an algebraic mapping, the singularity in the mapping is weaker; the derivatives of the Laplace solution with respect to the transformed variable are bounded (they even tend to 0). Fast convergence results (Orszag 1976).

The problem is due to the relatively slow decay of the irrotational component of the solution. This leads to the idea of subtracting this irrotational component in the hope that the remainder, or "vortical component," will be easier to approximate. Let us assume that as $y \to \infty$ the vorticity tends to 0 at least as fast as $\exp(-Ky)$ for some positive constant $K$: $|\omega| = O\big(exp(-Ky)\big)$, and examine the behavior of the velocity. The vertical velocity satisfies the Poisson equation

$$\hat{v}_{yy} - k^2\hat{v} = ik\hat{\omega}^+, \tag{14}$$

where $\hat{\omega}^+$ is the projection of the vorticity vector orthogonal to the $(\mathbf{k}, y)$ plane. Using (14) and (4) it can be shown that $\hat{v}$ has the form

$$\hat{v} = Ae^{-ky} + \hat{v}', \tag{15}$$

where $A$ is a constant and $\hat{v}' = O\big(exp(-Ky)\big)$. The point is that in most flows of interest, $K$ is much larger than $k$. Because of (11) and (15), $\hat{u}^+$ can be split as $\hat{v}$ was in (15). Finally, the $\hat{u}^-$ component itself is $O\big(exp(-Ky)\big)$, because it satisfies $\hat{u}^- = i\hat{\omega}_y/k$, where $\omega_y$ is the vertical component of vorticity.

Let us now express the results in terms of $\eta$. We shall assume that the functions are smooth in terms of $y$, and only consider the effect of the singularity in the mapping. Since $\exp(-Ky) = \eta^{Ky_0}$, a function that is $O\big(exp(-Ky)\big)$ is of class $C_n$ (has $n$ continuous derivatives) in terms of $\eta$ for any integer $n$ smaller than $Ky_0$. Thus if $Ky_0$ is large, the spectral method can approximate $\hat{v}'$ with a finite but high order of convergence (Gottlieb & Orszag 1977). If the function is $O\big(exp(-Ky)\big)$ for arbitrarily large values of $K$, infinite-order convergence is obtained. We conclude from (15) that, provided that the vorticity is $O\big(exp(-Ky)\big)$ for a large value of $K$ and that the error in the value of $A$ (the "subtraction error") is small enough, one can approximate boundary-layer velocity fields with an exponential mapping and polynomials, and obtain high-order convergence.

One can estimate the value of $K$ in some relevant flows. In Stokes' first problem and in Blasius flow, the mean vorticity is $O\big(exp(-Ky)\big)$ for arbitrarily large values of $K$ (Schlichting 1979). Thus the mean flow is approximated with infinite-order accuracy. In Stokes' second problem and in the laminar sink flow, $K$ is finite; $K^{-1}$ is of the order of the boundary-layer thickness. One may improve the accuracy by choosing $y_0$ so that $Ky_0$ is an integer, without having to make $y_0$ too large. In solutions of the Orr-Sommerfeld equation, $K$ is equal to $\sqrt{k(U_\infty - c)/2\nu}$, and is again much larger than $k$. The convergence to these solutions will be tested.

To use the property expressed in (15), the simplest strategy is to add to the family of basis functions one extra function per wave-vector, a function that behaves like $\exp(-ky)$ as $y \to \infty$, and to let the least-squares algorithm or the eigenvalue solver choose the value of $A$ along with the other coefficients. No separate effort is made to reduce the subtraction error. Including an extra function adds to the complexity of the program, and could disrupt the structure of the matrices built around the regular basis functions. However, this disruption is minimized by the fact that the irrotational component, by nature, is orthogonal to all the other basis functions. Thus it does not even add any extra bands or lines in the matrices. Only the + modes require the extra function. One minor problem is that if $ky_0$ happens to be an integer, the extra function is not linearly independent of the regular basis functions, which makes the matrix singular. If $ky_0$ is close to an integer or large (about 4), the matrix becomes ill-conditioned.

A method that incorporates a Laplace solution as an extra basis function is likely to be more accurate for the following reason. With the other methods, the slowly decaying irrotational component is described by the "regular" basis functions. This means that some resolution (collocation points) must be available at distances from the wall of the order of $k^{-1}$. With the present method, the extra function describes the irrotational component and no resolution by the regular functions is needed beyond the edge of the boundary layer (vortical region). In practice, $k^{-1}$, which is equal to $\Lambda/2\pi$ where $\Lambda$ is the period in the horizontal direction, is much larger than the boundary-layer thickness. The present method may not yield as good an *asymptotic* rate of convergence (when a large number of polynomials are used and the error is extremely small) as was shown by Boyd (1982). However, with a moderate number of polynomials it is significantly more accurate. When solving the Orr-Sommerfeld equation, a relative error of $10^{-6}$ in the phase velocity is obtained with about 25 polynomials. Orszag (1976) needed 42 Chebyshev polynomials to achieve the same accuracy (better accuracy could be obtained with the algebraic mapping by using only the odd Chebyshev polynomials, see Spalart 1984a).

A splitting into irrotational and vortical components may be beneficial even in a spectral method using an algebraic mapping, or in a finite-difference method, because it would allow one to bring almost all the points back into the boundary layer itself (in the finite-difference case, one would apply the condition $\hat{v}_y = -k\hat{v}$ at the edge of the domain, instead of $\hat{v} = 0$). The same ideas would apply to other unbounded flows; for instance, flows around solid bodies or vortex rings. In summary, if a flow has a region where the velocity field is both incompressible and irrotational, this region can and should be treated in a very economical fashion.

### 3.3. *Choice of the polynomials*

Let us consider the family of shifted Jacobi polynomials $G_n$ of degree $n$, defined on $[0,1]$ by $G_n(1) > 0$ and

$$\int_0^1 G_n(\eta)G_m(\eta)\eta d\eta = \frac{\delta_{nm}}{2(n+1)}, \tag{16}$$

where $\delta_{nm}$ is the Kronecker symbol. See the appendix for other properties of the $G_n$'s. We define the two families $h_n$ and $g_n$ by

$$h_n(\eta) \equiv (1-\eta)\eta G_n(\eta), \qquad g_n(\eta) \equiv (1-\eta)^2\eta G_n(\eta). \tag{17}$$

The $h_n$ polynomials have a single zero at the wall and will be used for $\hat{u}^-$; the $g_n$ polynomials have a double zero and will be used for $\hat{v}$. Both $h_n$ and $g_n$ tend to 0 as $y$ tends to $+\infty$. As shown in the appendix, $h_n$, $g_n$ and the required derivatives can be expressed as combinations of a few polynomials of the type $\eta G_m$. As a result, the matrices involved in (8) are banded, with five and nine bands for the $h_n$'s and the $g_n$'s, respectively. The extra basis function, $g_{-1}$, is defined by

$$g_{-1}(\eta) = 3\eta^{ky_0} + (ky_0 - 4)\eta G_0 + (1 - ky_0)\eta G_1. \tag{18}$$

It has a double zero at the wall and is orthogonal to the regular basis functions, except for the few that involve $G_0$ or $G_1$. Figure 1 is a plot of the first few $g_n$ functions versus $y$, with $ky_0 = 0.4$. The extra function $g_{-1}$ stands out for large values of $y$. As $n$ increases $g_n$ has more and more zeroes within $[0,\infty]$; the position of the zeroes roughly indicates the

region where good resolution is available. The collocation points are indicated by crosses on the axis. They are seen to cluster near the wall, and to be very sparse for $y$ beyond about $5y_0$.

The mean component, with $\mathbf{k} = (0,0)$, requires special treatment. Both horizontal components are treated as $-$ modes, using the $h_n$ functions, and $\hat{v} = 0$ (Moser *et al.* 1983). In addition, to obtain different values at $y = 0$ and for $y \to \infty$ in accordance with (3) and (4), the function $U_\infty(1-\eta)$ is added to the expansion in the $\mathbf{k} = (0,0)$ mode. This requires a simple correction in the viscous term.

### 3.4. *Accuracy tests*

The accuracy of the method was first tested by approximating typical mean velocity profiles: the solutions to Stokes' first problem, the Blasius equation, and the laminar sink flow. The reference solution for the Blasius equation was obtained by fourth-order Runge-Kutta integration with a large number of steps. The relative error in the slope at $y = 0$ is plotted in figure 2 as a function of the number of polynomials. Very fast convergence is observed for the first two cases; the convergence is only moderately fast for the sink flow, which confirms the analysis. These tests did not involve the extra function.

The Orr-Sommerfeld equation was also solved; the extra function is now involved. Figure 3 is a plot of the spectrum for the Blasius flow at its critical condition ($R_{\delta^*} = 519.06381$ and $k\delta^* = 0.303773$) with 26 and 53 polynomials. The complex velocities $(c_r, c_i)$ are plotted; $c_r$ gives the phase velocity and $c_i$ gives the growth rate. The principal eigenvalue is neutrally stable. Its convergence is also described in figure 2 and is very fast. This indicates, empirically, that even with the simple strategy that was adopted, the subtraction error is very small. The best value of $y_0$ is about $2\delta^*$. The convergence without the extra function $g_{-1}$ is also plotted for comparison and is much slower, as one would expect.

In addition to a few discrete eigenvalues, the numerical spectra in figure 3 show a string of eigenvalues that starts at the point with complex velocity (1,0) and extends to large negative values of the imaginary part. As the number of polynomials is increased this string becomes denser and slowly converges to the $c_r = 1$ axis. Grosch & Salwen (1978) showed that the exact spectrum includes a continuous line on that axis, and that the corresponding eigenfunctions behave like sine waves as $y \to \infty$. Such functions cannot be well approximated by the basis functions that were chosen, since these tend to 0 as $y \to \infty$ (figure 1). This explains why the convergence to the continuous part of the spectrum is so slow. These eigenfunctions are not relevant since they do not satisfy (4). In any case the representation of the continuous spectrum, while not very accurate, is not abnormal.

### 3.5. *Gaussian quadrature and aliasing removal*

The solution of the momentum equation (8) requires the evaluation of various integrals. Integrals of the type $< \mathbf{U}, \mathbf{V} >$ and $< \nabla\mathbf{U}, \nabla\mathbf{V} >$ are computed exactly using the definition of $g_n$ and $h_n$ (17), and the properties of the $G_n$ polynomials (16). The integral $< \mathbf{U} \times \omega, \mathbf{V} >$ is evaluated by Gaussian quadrature in real space, which is computationally more efficient than a convolution sum in spectral space. In each Fourier direction the quadrature points are equally spaced and the number of points is 3/2 times the number of wave-numbers, so that the quadrature of the product $(\mathbf{U} \times \omega).\mathbf{V}$ is exact. In the polynomial direction the quadrature points and weights are computed using the method described by Golub & Welsch (1969). Again, the number of points is 3/2 as large as the number of polynomials and the quadratures are exact. The aliasing errors are removed. It is essential to use the $(\mathbf{U} \times \omega)$ form of the transport term; the other expression, $(\mathbf{U}.\nabla\mathbf{U}).\mathbf{V}$, would

not tend to 0 fast enough as $y \to \infty$ to be integrated properly.

The use of the "3/2 rule" is relatively expensive and it is a matter of controversy whether aliasing removal is actually necessary. Tests were conducted, in which a fully developed turbulent field was produced using the program with de-aliasing (Spalart & Leonard 1985). The integration in time was then continued without de-aliasing (which reduced the computer work per time step by about 40%). However, the turbulent energy quickly started to decay and after a few hundred time steps, the turbulence was clearly "dying." In some applications of spectral methods, the solutions may be resolved well enough for aliasing errors to be harmless. In the present case de-aliasing is necessary. It is not clear how aliasing errors disturbed the flow. One of the first symptoms was that the energy of the high spanwise wave-numbers increased significantly when compared with the initial spectrum. The problem cannot be that the global kinetic energy is affected, because one can show that it is semiconserved even with aliasing; it is more likely that the partition of the energy between low and high wave-numbers is affected.

### 3.6. *Time integration*

Equation (8) is integrated in time using a hybrid scheme. The viscous term $-\nu < \nabla\mathbf{U}, \nabla\mathbf{V} >$ is better treated by an implicit scheme, in order to obtain stability in spite of its "stiffness." The second-order-accurate Crank-Nicolson scheme is used. On the other hand, the transport term $< \mathbf{U} \times \omega, \mathbf{V} >$ is not easily treated by an implicit scheme, because it is hard to linearize with a spectral method. In addition, it is less stiff than the viscous term since it involves only one first derivative. This leads one to treat the transport term by an explicit scheme. A low-storage third-order-accurate scheme was derived by A. Wray (personal communication 1983). This scheme uses three substeps; the first one amounts to an Euler explicit step, while the second and the third amount to Adams-Bashforth steps, but with uneven substeps and weighting coefficients. The global scheme is equivalent to the classical third-order Runge-Kutta scheme when applied to linear equations; the stability limit expressed as a Courant number is $\sqrt{3}$. In practice, the Courant number is evaluated as

$$\frac{2\pi}{3}\Delta t\left(\frac{|u|}{\Delta x} + \frac{|v|}{\Delta y} + \frac{|w|}{\Delta z}\right), \tag{19}$$

where $\Delta x$, $\Delta y$, and $\Delta z$ are the spacing between collocation points. This definition of the Courant number is the correct one for the Fourier directions. The definition in the $y$ direction was done purely by analogy. During a simulation the time step $\Delta t$ is automatically adjusted so that the maximum local Courant number is $\sqrt{3}$. Typically, because of the viscous dissipation and the intermittent character of the velocity field, numerical instability does not occur until the Courant number limit is set to at least 2.3. The extra term $\mathbf{f}$ in (2), if present, is treated by the explicit scheme along with the transport term. This term is small and does not cause any stability problems.

Since the treatment of the viscous term is second-order accurate, the overall accuracy is only of second order. The third-order scheme does not improve the formal accuracy, but in practice it significantly improves both the accuracy and the stability (as compared with the commonly used Adams-Bashforth second-order scheme) and its numerical dissipation is moderate. An additional improvement is gained by doing the time integration in a Galilean reference frame that is "sliding" at a velocity $c$ with respect to the wall. This reduces the value of $|u|$ in (19), which allows longer time steps and improves the accuracy. For transition simulations (see Part 2), $c$ is chosen to be the phase velocity of the primary

Tollmien-Schlichting wave. Thus the wave is standing in the sliding frame, and is followed very accurately. For turbulence simulations (see Part 3), $c$ is taken as $U_\infty/2$. There is not as much gain, because in these simulations $\Delta y$ is so small that the main contribution to the Courant number comes from the $v$ component.

### 3.7. *Resources*

The program runs on a Cray X-MP computer and is written in the VECTORAL language (A. Wray, personal communication 1983). The algorithm alternates between two "passes" through the data base. During the "horizontal pass," the Fourier transforms and the $\mathbf{U} \times \omega$ products are computed $(x, z)$ plane by $(x, z)$ plane. During the "vertical pass," the Jacobi transforms, the Stokes matrices, and their Cholesky decomposition are computed $(k_x, y)$ plane by $(k_x, y)$ plane. This allows one to use secondary storage and access only a few planes at a time. About 40% of the computing time is used by Jacobi transforms, 40% by Fourier transforms, and 20% by the matrix inversions. Transition simulations, with $16 \times 40 \times 48$ collocation points in $x$, $y$ and $z$, use about $3 \times 10^5$ words of storage and 2.7 seconds of CPU time per complete time step. Each run takes a few hundred time steps. Typical turbulence simulations, with $192 \times 45 \times 128$ points, use about $10^6$ words of core memory, $1.7 \times 10^6$ words of secondary storage (two words being packed into one before writing to disk), and 18 seconds per step. A fully developed turbulent field is obtained in a few thousand steps.

Since the turbulence is highly inhomogeneous and anisotropic, choosing the number of points to be used in each of the three directions is not trivial. Given a total number of points, one would like the simulation to be balanced, and not to see the accuracy be limited by one of the directions while another one is overresolved. One may examine the one-dimensional spectra, but spectra represent a large amount of information and one would like to have a simple, objective indicator of how good the resolution is in each direction. In addition, spectra are not available in the polynomial direction.

One possibility is to consider how well correlated the solution is between a grid point and its immediate neighbors. For small separations the correlation is directly related to the Taylor micro-scale $\lambda$, so that it would be roughly equivalent to consider the ratio $\Delta/\lambda$. $\Delta$ is the distance between grid points. Let $C_x$ be defined by

$$C_x(y) \equiv \frac{\overline{\mathbf{U}'(x).\mathbf{U}'(x+\Delta x)}}{\overline{|\mathbf{U}'|^2}}, \tag{20}$$

where $\mathbf{U}'$ is the fluctuating velocity vector, and $C_y$ and $C_z$ be defined similarly. The bars denote averages taken in the homogeneous directions, $x$ and $z$, so that $C_x$, $C_y$, and $C_z$ are functions of $y$. By comparing these three functions directly, one is implicitely assuming that the "resolving power" per grid point is the same in all directions, which is plausible with a fully spectral method. With a mixed spectral/finite-difference method, for instance, one would have to "penalize" the finite-difference direction.

The correlations in a typical turbulent simulation are shown in figure 4. The closer the correlation is to 1, the better the resolution is. The values of the three correlations are comparable; the simulation was reasonably well balanced. As expected, $C_x$ and $C_z$ worsen near the wall, because the length scales decrease while $\Delta x$ and $\Delta z$ do not. On the other hand, $C_y$ improves near the wall, presumably because $\Delta y$ decreases faster than the length scales of the flow. This suggests that the Jacobi polynomials gather more than enough points near the wall. Ideally $C_y$ would be independent of $y$. This also suggests

that Chebyshev polynomials, which gather even more points near the wall, may be less efficient than Jacobi polynomials for the flows we are simulating.

A comparison of the two-point correlations cannot give a rigorous proof that the resolution is optimally distributed, but it gives a simple and convenient estimate of the accuracy, and helps one choose values for the major numerical parameters: $N_x$, $N_y$, $N_z$, and $y_0$. The correlations are responsive to changes in resolution; refining the grid by a factor of 2 reduces the "lack of correlation" $1 - C$ roughly by a factor of 4. The correlation curves may also be used to estimate the relative accuracy of separate simulations, for instance at different Reynolds numbers.

The author had useful discussions at NASA Ames Research Center with Drs. J. Kim, A. Leonard, P. Moin, R. Moser, R. Rogallo and A. Wray. He thanks Dr. D. Jespersen for reviewing the manuscript, and Mr. H. Lomax for his teaching and his support.

## Appendix

This appendix outlines the construction of the basis functions. The properties of the Jacobi polynomials that were used are the following. The two properties $G_n(1) > 0$ and (16) fully define the $G_n$ family. These polynomials satisfy $G_n(1) = 1$ and are described by Abramowitz & Stegun (1972) (with a slightly different normalization). The actual building blocks are the polynomials $\eta G_n$, which satisfy

$$\int_0^\infty (\eta G_n)(\eta G_m) dy = \frac{y_0 \delta_{nm}}{2(n+1)} \tag{A1}$$

since $dy = -y_0 d\eta/\eta$. Abramowitz and Stegun also give the recursion relationship,

$$\eta G_n = \frac{n+2}{2(2n+3)} G_{n+1} + \frac{2(n+1)^2}{(2n+1)(2n+3)} G_n + \frac{n}{2(2n+1)} G_{n-1}, \tag{A2}$$

and the differentiation relationship,

$$\eta(1-\eta)\frac{dG_n}{d\eta} = -\frac{n(n+2)}{2(2n+3)} G_{n+1} - \frac{n(n+2)}{(2n+1)(2n+3)} G_n + \frac{n(n+2)}{2(2n+1)} G_{n-1}. \tag{A3}$$

The functions $h_n$ and $g_n$ being defined by (17), (A2) and (A3) allow one to express $h_n$ and $g_n$, as well as $h_n$'s first derivative and $g_n$'s first two derivatives, in terms of the $\eta G_m$'s. Higher derivatives are not needed when using Leray's formulation. For instance

$$h_n = -\frac{(n+2)}{2(2n+3)} \eta G_{n+1} + \frac{2n^2+4n+1}{(2n+1)(2n+3)} \eta G_n - \frac{n}{2(2n+1)} \eta G_{n-1}, \tag{A4}$$

$$\frac{dh_n}{dy} = \frac{1}{y_0}\left[\frac{(n+2)^2}{2(2n+3)} \eta G_{n+1} + \frac{(n+1)^2}{(2n+1)(2n+3)} \eta G_n - \frac{n^2}{2(2n+1)} \eta G_{n-1}\right]. \tag{A5}$$

Note that the multiplication by $(1-\eta)$ in (17), which was done to enforce the boundary condition, fortuitously improves the expression of the derivative as it did for Chebyshev polynomials in the Moser *et al.* (1983) method. Equations (A1), (A4) and (A5) allow one to compute the matrices representing the first and third term of (8) for the - modes. Both matrices are pentadiagonal. The algebra is very similar for the $g_n$ functions.

## REFERENCES


**Abramowitz, M. & Stegun, I. A. 1972** Handbook of mathematical functions. National Bureau of Standards Appl. Math. Series 55.

**Boyd, J. P. 1982** The optimization of convergence for Chebyshev polynomial methods in an unbounded domain. *J. Comp. Phys.* **45, 1**, 43-79.

**Cain, A. B., Ferziger, J. H. & Reynolds, W. C. 1984** Discrete orthogonal function expansions for non-uniform grids using the Fast Fourier Transform. *J. Comp. Phys.* **56, 2**, 272-286.

**Golub, G. H. & Welsch, J. H. 1969** Calculation of Gauss quadrature rules. *Math. of Comp.* **29**, 221-230.

**Gottlieb, D. & Orszag, S. A. 1977** Numerical analysis of spectral methods. NSF-CMBS Monograph 26, Soc. Ind. and Appl. Math., Philadelphia, Penn.

**Grosch, C. E. & Orszag, S. A. 1977** Numerical solution of problems in unbounded regions: coordinate transformations. *J. Comp. Phys.* **25**, 273-296.

**Grosch, C. E. & Salwen, H. 1978** The continuous spectrum of the Orr-Sommerfeld equation. Part 1. The spectrum and the eigenfunctions. *J. Fluid Mech.* **87, 1**, 33-54.

**Heywood, J. G. 1980** The Navier-Stokes equations: On the existence, regularity and decay of solutions. *Indiana Univ. Math. J.* **29, 5**, 639-681.

**Kleiser, L. 1982** Spectral simulations of laminar-turbulent transition in plane Poiseuille flow and comparison with experiments. $8^{th}$ Int. Conf. on Num. Meth. in Fluid Dyn., Aachen, June 1982.

**Ladyzhenskaya, O. A. 1969** The mathematical theory of viscous incompressible flow. $2^{nd}$ ed. Gordon and Breach, New York.

**Leonard, A. 1981** Divergence-free vector expansions for 3-D flow simulations. *Bull. Amer. Phys. Soc.* **26**, 1247.

**Leonard, A. & Wray, A. 1982** A new numerical method for the simulation of three-dimensional flow in a pipe. $8^{th}$ Int. Conf. on Num. Meth. in Fluid Dyn., Aachen, W. Germany, June 1982.

**Marcus, P. 1984** Simulation of Taylor-Couette flow. Part 1. Numerical methods and comparison with experiment. *J. Fluid Mech.* **146**, 45-64.

**Moin, P. & Kim, J. 1982** Numerical investigation of turbulent channel flow. *J. Fluid Mech.* **118**, 341-377.

**Moser, R. D. Moin, P. & Leonard, A. 1983** A spectral numerical method for the Navier-Stokes equations with applications to Taylor-Couette flow, *J. Comp. Phys.* **52**, 524-544.

**Orszag, S. A. 1976** Numerical simulation of turbulent flow over a compliant boundary. Report 63, Flow Research Inc., Kent, Wash.

**Orszag, S. A. & Kells, L. C. 1980** Transition to turbulence in plane Poiseuille and plane Couette flow. *J. Fluid Mech.* **96**, 159-205.

**Orszag, S. A. & Patera, A. T. 1983** Secondary instability in wall-bounded shear flows. *J. Fluid Mech.* **128**, 347-385.

**Rogallo, R. S., & Moin, P. 1984** Numerical simulation of turbulent flows. *Ann. Rev. Fluid Mech.* **16**, 99-138.

**Schlichting, H. 1979** Boundary layer theory, $7^{th}$ ed., McGraw-Hill, New York.

**Spalart, P. R. 1984a** A spectral method for external viscous flows. *Contemp. Math.* **28**, 315-335. J. E. Marsden, Ed. American Math. Soc., Providence, Rhode Island.

**Spalart, P. R. 1984b** Numerical Simulation of Boundary-Layer Transition. $9^{th}$ Int. Conf. on Num. Meth. in Fluid Dyn., Paris, June 1984.
**Spalart, P. R. & Leonard, A. 1985** Direct numerical simulation of equilibrium turbulent boundary layers. Proceedings of the $5^{th}$ Symposium on Turbulent Shear Flows, Ithaca, USA, August 7-9, 1985.
**Temam, R. 1983** Navier-Stokes equations and non-linear functional analysis, NSF-CMBS Monograph 41, Soc. Ind. and Appl. Math., Philadelphia, Penn.
**Wray, A. & Hussaini, M. Y. 1984** Numerical experiments in boundary layer stability. *Proc. Roy. Soc. London* **A 392**, 373-389.

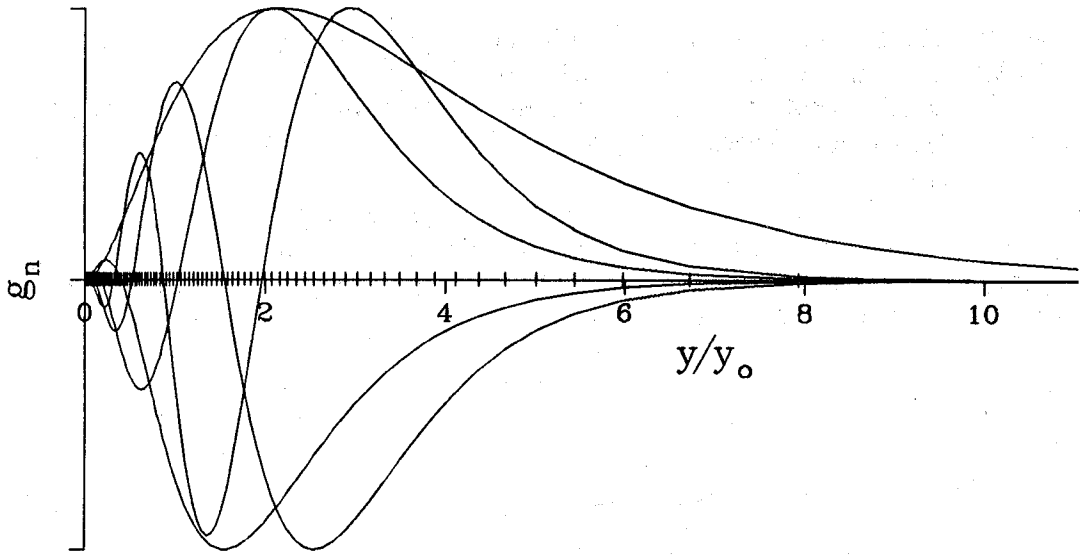


Figure 1. Basis functions $g_{-1}$ to $g_3$ and collocation points.

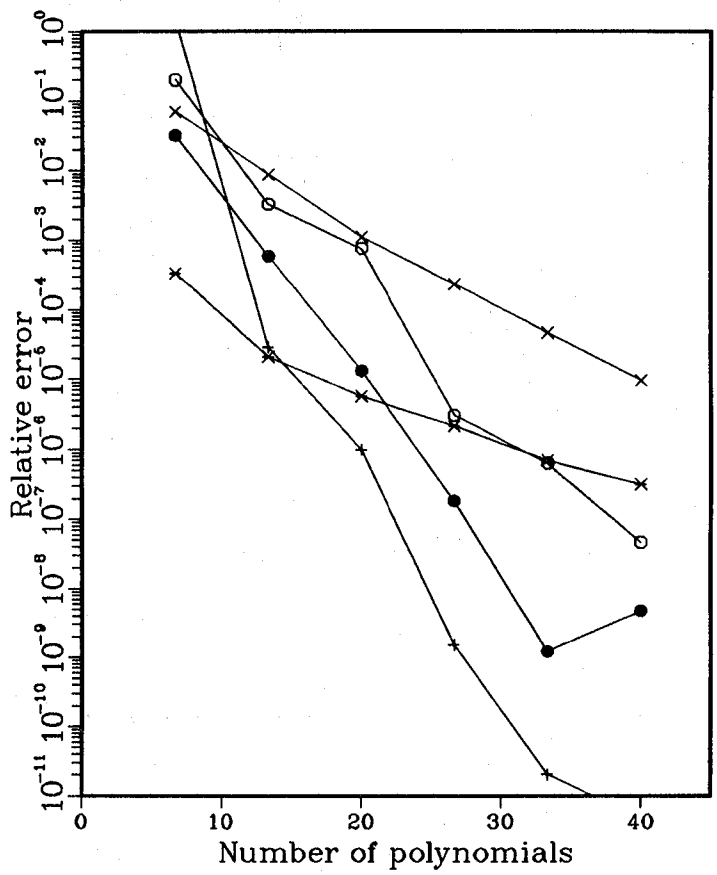


Figure 2. Relative error in numerical solutions, as a function of the number of polynomials. • Stokes layer; o Blasius layer; * Sink Flow; + Orr-Sommerfeld equation, using $g_{-1}$; × Orr-Sommerfeld equation, omitting $g_{-1}$.

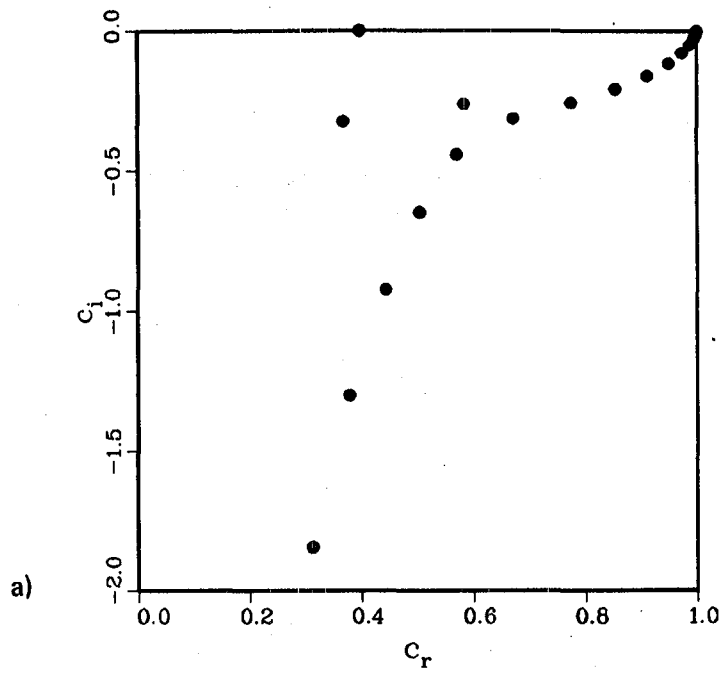


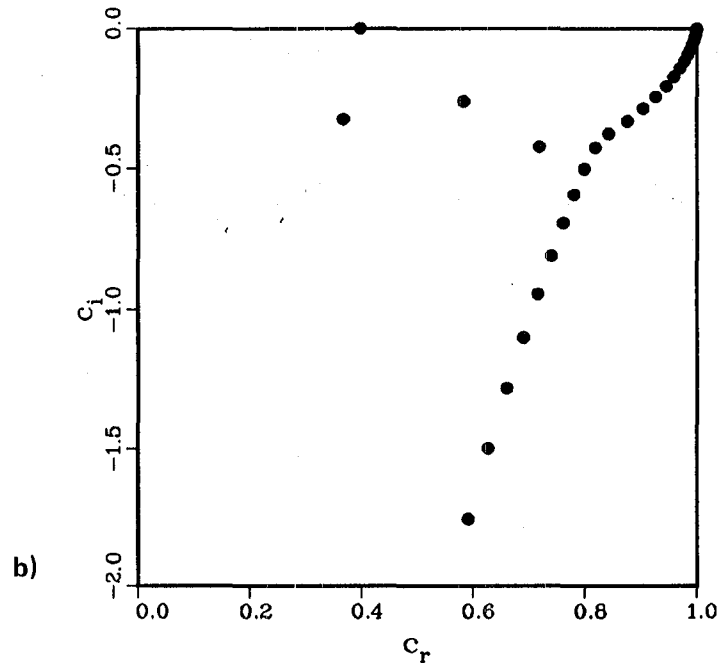


Figure 3. Spectrum of Orr-Sommerfeld equation. a) with 26 polynomials; b) with 53 polynomials.

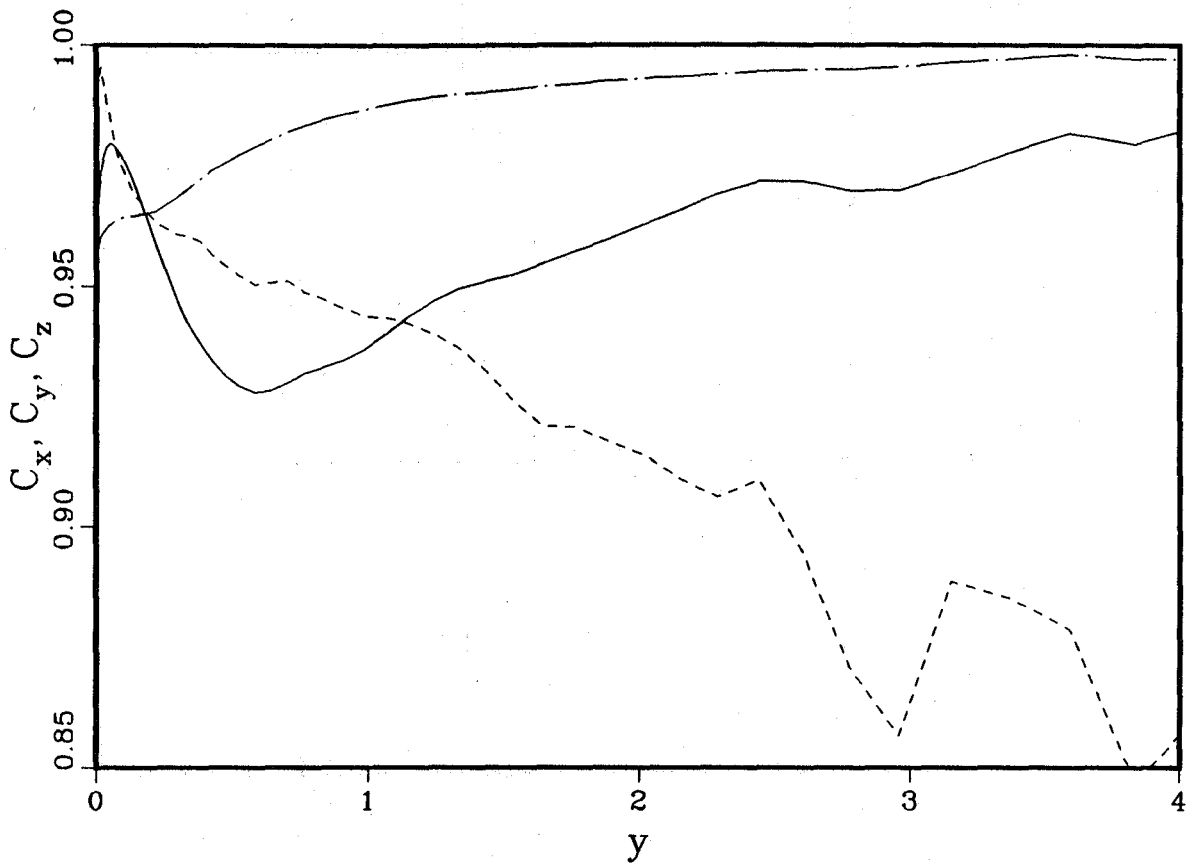


Figure 4. Two-point correlations in a turbulent boundary layer. — $x$ direction; - - - $y$ direction; - — - $z$ direction.

| 1. Report No. | 2. Government Accession No. | 3. Recipient's Catalog No. |
|---|---|---|
| NASA TM-88222 | | |

| 4. Title and Subtitle | 5. Report Date |
|---|---|
| NUMERICAL SIMULATION OF BOUNDARY LAYERS. PART 1. WEAK FORMULATION AND NUMERICAL METHOD | February 1986 |
| | 6. Performing Organization Code<br>RFT |
| 7. Author(s)<br>Philippe Spalart | 8. Performing Organization Report No.<br>A-86029 |
| 9. Performing Organization Name and Address<br>Ames Research Center<br>Moffett Field, CA 94035 | 10. Work Unit No.<br><br>11. Contract or Grant No. |
| 12. Sponsoring Agency Name and Address<br>National Aeronautics and Space Administration<br>Washington, DC 20546 | 13. Type of Report and Period Covered<br>Technical Memorandum<br>14. Sponsoring Agency Code |

15. Supplementary Notes

Point of Contact: Philippe R. Spalart, Ames Research Center, M/S 202A-1, Moffett Field, CA 94035 (415) 694-6667 or FTS 464-6667

16. Abstract

A numerical method designed to solve the time-dependent, three-dimensional, incompressible Navier-Stokes equations in boundary layers is presented. The fluid domain is the half-space over a flat plate, and periodic conditions are applied in the horizontal directions. The discretization is spectral. The basis functions are divergence-free and a weak formulation of the momentum equation is used, which eliminates the pressure term. An exponential mapping and Jacobi polynomials are used in the semi-infinite direction, with the irrotational component receiving special treatment. Issues related to the accuracy, stability and efficiency of the method are discussed. Very fast convergence is demonstrated on some model problems with smooth solutions. The method has also been shown to accurately resolve the fine scales of transitional and turbulent boundary layers.

| 17. Key Words (Suggested by Author(s)) | 18. Distribution Statement |
|---|---|
| Numerical simulation<br>Boundary layers<br>Transition<br>Turbulence | Unlimited<br><br>Subject category - 34 |

| 19. Security Classif. (of this report) | 20. Security Classif. (of this page) | 21. No. of Pages | 22. Price* |
|---|---|---|---|
| Unclassified | Unclassified | 20 | A02 |

*For sale by the National Technical Information Service, Springfield, Virginia 22161

**End of Document**